INTERNATIONAL JOURNAL OF SUSTAINABLE CONSTRUCTION ENGINEERING AND TECHNOLOGY
VOL. 14 NO. 1 (2023) 202-216

IJSCET

http://publisher.uthm.edu.my/ojs/index.php/ijscet

ISSN : 2180-3242 e-ISSN : 2600-7959

International Journal of Sustainable Construction Engineering and Technology

Influence of Near Fault Earthquakes with Forward Directivity and Fling Step on Seismic Response of Steel Box-Girder Bridge

Mirza Aamir Baig[1*], Md. Imteyaz Ansari[1], Nazrul Islam[1], Mohammad Umair[1]

[1]Department of Civil Engineering,
Jamia Millia Islamia University, New Delhi, 110025, INDIA

*Corresponding Author

DOI: https://doi.org/10.30880/ijscet.2023.14.01.018
Received 26 August 2022; Accepted 08 January 2023; Available online 14 February 2023

Abstract: The existing bridge seismic design guidelines that rely on the ground acceleration in the far fault zone, ignore the potential impact of near fault forward directivity and fling-step effects on the bridge structures. In the current study probabilistic seismic damage evaluation of a continuous four-span box girder bridge under the impact of near-fault forward directivity and fling step effect is studied employing the fragility analysis. The incremental dynamic analysis is used to construct the fragility curves which shows a range of damage states from minor to collapse for the different damage metrics and for the considered peak ground acceleration varying between 0.1g and 1.2g. Damage metrics such displacement pier ductility, rotational pier ductility and displacement of girder are used to develop the fragility curves and the probabilistic seismic damage model. To evaluate the bridge vulnerability, a probabilistic seismic damage assessment is performed using an ensemble of forward directivity and an ensemble of fling-step comprising permanent ground offset. The suggested probability-based earthquake damage framework is anticipated to be a well-versed model able to estimate the seismic damages to the continuous box girder bridges while taking into account the variation of near fault earthquakes. The findings show that, even at low PGA values the forward directivity and the fling-step ground motions represent a significant risk to the bridge.

Keywords: Near fault earthquake, fragility curve, probabilistic seismic demand, forward directivity, fling step

1. Introduction

A robust bridge that can withstand extreme loading conditions such as an earthquake is a valuable addition to any transportation system. Highway bridges must be evaluated for seismic susceptibility in order to be prepared for physical and economic damage caused by earthquakes. In prior earthquakes across the world, bridges have been shown to be one of the most crucial highway transportation components. The bridge damage assessment model has been developed with outmoded governing norms (Mangalathu et al., 2019). The damaging aspects of near fault earthquakes are ignored by the current bridge seismic design specifications, which were established for far-fault earthquakes. Although there have been quite a few near-fault seismic occurrences recently, their effects on the bridges have not yet been fully investigated.

*Corresponding author: aamirmirzagarri@gmail.com

Near-field ground motion could have a significant effect on structure responses, especially in long-period structure systems. In a velocity-time history, near-fault seismic data may contain impulsive ground motions (Ertuncay et al., 2021). Long-period pulses in near fault earthquakes have a higher damage potential, especially for flexible structures like bridges. In near fault earthquakes that cause significant structural damage, velocity pulses of large-amplitude and long-period are detected in the ground motion time history plots. Such features include the fling-step impact in the fault-parallel plane and the forward-directivity impact in the fault-normal plane (Yadav & Gupta, 2017).

These two features can put a lot of strain on structures, requiring them to disperse a lot of energy with only a few major displacement excursions. A directivity pulse results from the fault propagating at about the same velocity as the shear wave. During an earthquake, this pulse can induce significant damage if it is apparent in the rupture forward direction once the frequency of the structure is near to the pulse. Such well-known examples include the 1992 Landers, 1999 Kocaeli, 1999 Chi-Chi, and 2011 Tohoku (Hamidi et al., 2020). Fling happens when the ground shifts permanently in the event of an earthquake, because accelerometer ground motion recordings include defects that make measuring static offsets difficult, it is frequently neglected.

There are fewer relevant investigations because the fling-step characteristic data in ground motion is scarce and difficult to extract. In the Chi-Chi earthquake, the surface rupture due to large permanent ground displacement was devastating and the structures that crossed or were close to a fault line suffered catastrophic destruction (Burks & Baker, 2016).

Forward-directivity pulses influence near-field ground motions, resulting in substantial velocity pulses in which the majority are related to faults in normal direction. The long-period coherent component of ground vibrations is amplified by the directivity pulses, which can be seen in the time histories of displacement and velocity, as well as the corresponding response spectra (Mimoglou et al., 2017). An automatic classification for detecting velocity pulse-like ground motion for the Wenchuan earthquake was proposed within a 100 km rupture distance. This could help researchers investigate the bridge damage mechanisms subjected to near-field earthquakes (Gentile & Galasso, 2021). Near-fault pulses, such as ground vibrations, have more severe effects on bridges in both directions than far-fault pulses. Also, looking at how different bridges react shows that irregular bridges are the most likely to be damaged by near-fault earthquakes. The majority of structures that were already in existence and built before the 2008 implementation of the new design codes, as well as the seismic risk map, which allocates a PGA to previously non-seismic sites, is a major source of concern in Italy (Lo Monte et al., 2018).

Near-field ground motion with directivity pulses and fling-step features is used to investigate an RC bridge pier. The effects of various earthquake ground variables on bridge performance, like average period, orientation and arias intensity are explored (Sengupta et al., 2016). The performance of the bridge due to impulsive ground motion for the bridge is observed to be greater than non-impulsive ground motion. The seismic sensitivity of the girder and bent for near-field impulsive vibrations is higher.

Vulnerability of bridges to near-field earthquakes is a severe issue in Italy because most existing structures were built prior to the 2008 national building code and earthquake hazard map, which allocates a non-zero peak ground acceleration (PGA) to previously non seismic sites. The presence of three different deck types (tub girder, reinforced concrete T-beam and prestressed concrete beam) as well as geometrical and economic constraints (limited deck-to-deck gaps and bearing heights) were all crucial factors (Lo Monte et al., 2018).

The experience from past seismic events is seen in the way seismic design codes, bridge details, and building practices in different countries change over time. The seismic code for building highway bridges has evolved significantly as a result of the Indian subcontinent's history of devastating earthquakes. Bridges made using so many different design methods need to be looked at to see how vulnerable they are to future earthquakes. But there aren't any of these kinds of frameworks for evaluating how vulnerable highway bridges are to earthquakes in the country. Using fragility curves, this study looks at how the rules of seismic codes affect how well a bridge works during an earthquake and how likely it is to collapse. When seismic design principles are used to build the case study bridge, its performance is much better than when it was not designed for earthquakes (Somerville et al., 1997).

The preceding literature review demonstrates that existing bridge seismic design guidelines that rely on ground acceleration in the far field, ignore the potential impact of fling-step and pulses from forward directivity. In this work, nonlinear time history analysis is used to investigate the seismic risk of a steel box girder bridge with near-field forward directivity and fling-step seismic action. CSI Bridge develops a reference bridge that exhibits the fundamental properties of continuous steel box girder bridges. The pier ductility and maximum deck displacement are taken as demand, whereas the peak ground acceleration (PGA) is considered a seismic intensity variable. Linear log-log regression analysis is used to create probabilistic seismic demand model for bridge components. The bridge vulnerability is assessed using established probabilistic seismic demand models and fragility curves.

2. Near Fault Earthquakes

An earthquake happens when a fault suddenly ruptures and slips because this causes the stored energy to be released in the form of seismic waves, which in turn cause the earth to shake. Ground motions in the near fault zone frequently exhibit a variety of characteristics, each of which is capable of having a significant influence on the response of structures. In the direction of the fault normal, this results in an effect known as "forward-directivity" and in the direction of the fault parallel this results in a permanent displacement known as the "fling step" (Mena & Mai, 2011). When a site is located in the near-field region of a fault, the characteristics of the ground motion at the site are determined by the rupture propagates in relation to the site.

The rupture spreads in two dimensions along the fault plane after it originates at the hypocenter and moves outward. If the rupture moves in the direction of the site, then we say that the site is located in the forward directivity area. At the beginning of the velocity time series experience a pulse with a short duration and a large amplitude in the direction that is perpendicular to the fault plane. If the rupture propagates away from the location and records a moderate amplitude ground motion with a long duration in the fault's normal direction the location is considered to be in the backward directivity area of the fault zone (Moniri, 2017). Sites with forward directivity experience multiple cycles of substantial amplitude velocity pulses in the direction of the fault, whereas records made with backward directivity do not show any movements that resemble pulses. This particular type of earthquake is characterized by a pulse in the velocity time history in the direction that is normal to the fault line, and it typically takes place in an area that is not too far from the fault line (Bolt, 2004).

In the event that an earthquake occurs along a fault, the two sides of the rupturing fault will shift relative to one another, which will result in permanent ground tectonic deformation. This deformation, also known as the fling step, can occur regardless of the particulars of the source rupture velocity (Bhagat et al., 2021).

The fling step is characterized by a unidirectional monotonic step that is associated with a large-amplitude velocity pulse. This step is the result of residual ground displacement that was caused by tectonic deformation that was linked with the rupture event. When the earth is permanently moved as a result of a rupture caused by seismic activity, this phenomenon is known as fling-step. The one-sided dominant velocity pulse that is characteristic of fling-step characteristics is what causes the displacement time-history to take on the form of a monotonic step (Nicknam et al., 2014).

The most well-known near-field earthquakes with the two characteristics stated are Chi-Chi, which occurred in Taiwan in 1999; Kocaeli, which occurred in Turkey in 1999; and Landers, which occurred in the United States in 1992.

3. Probabilistic Seismic Damage Analysis

In the event of an earthquake, the fragility curves are used to forecast the probable damage of the structure. These curves serve as an indication to determine the amount of physical damage that has been occurred to the structure during seismic risk evaluations. Fragility curves have developed into crucial decision-making tools for evaluating seismic vulnerability of the bridge structures which is close to the fault. The fragility curves are the result of a parameter that describes the intensity measure, and they show the probability that the engineering demand variable (EDV) of a structure will exceed the specified damage state (DS) (Billah et al., 2013). When evaluating the performance of the bridge physical components, damage probability models or fragility functions are developed to quantify the damage level of the bridge components under specified ground motions. These fragility curves provide a visual representation of the possibility of structural damage resulting from a variety of different forms of ground shaking. In addition, they suggest that there is a connection between earthquake shaking and the degree of damage. The generation of fragility curves may be achieved through the use of either a numerical simulation of different nonlinear time histories or an empirical technique that is based on the data that is accessible (Fariborz & Vahid, 2004). The exceedance probability (P) for a given intensity level (IL) can be computed by taking the ratio of the number of situations (Ni) in which the damage measure (DM) is greater than or equal to the threshold damage state (Dsi) to the total number of cases (Nc). Cumulative distributions based on the normal or log-normal distribution can be used to depict IDA fragility curves (Muntasir Billah & Shahria Alam, 2015).

3.1 Damage Model

In a mathematical formulation, the probabilistic seismic demand model (PSDM) combines the ground motion intensity measure with the structural demand index. With the use of this process, the demand value for a certain IL may be determined. An incremental dynamic analysis dataset for a particular ground-motion ensemble, using the bridge as an example, reveals the correlation between the intensity measure parameter and the engineering demand variable (EDV) (Zeng et al., 2019). In order to determine the model variables and standard deviation the dataset must include the nonlinear dynamic analysis (NDA) result derived from the ground-motion recordings. The strip-based and cloud-based procedures both involve a series of time-

history investigations, including non-linear dynamic analyses of a particular structure under the effect of a collection of ground motion data. With ten values for each seismic ensemble, the strip-based technique is used, which is one of the easiest ways to represents bridge response data (Ma et al., 2016).

The 240 data pairs represented by EDPs and IMs are the result of a nonlinear time-history analysis of the ensemble of ground motions. The conditional mean of the engineering demand parameter for a given intensity measure may be considered to be linear in log-log space if the EDP distribution is lognormal and the conditional dispersion can be assumed to be constant.

Based on threshold damage limit levels, seismic damage is divided into four damage states, namely: minor, moderate, severe and collapse (Baker & Cornell, 2008).

It is assumed that the fragility function has a log-normal distribution and may be represented by the following equations:

$$P[LS/IM=X] = \Phi\left((lnx - \mu)/\beta\right) \quad (1)$$

where P [LS/IM] represents the probability of exceeding the damage threshold limit for a particular ground motion intensity measure, X represents ground motion in relation to peak ground acceleration (PGA), μ and β denotes the median of ln X and standard deviation, as well as the cumulative normal distribution function. The structural response variable (EDP) indicates the variation in damage measure induced by earthquake ground motions (Federal Emergency Management Agency, 2020).

$$\beta_{total} = \sqrt{\beta_D{}^2 + \beta_C{}^2} \quad (2)$$

The fragility curves were generated by the use of an analytical technique known as incremental dynamic analysis. The response distribution is lognormal, and the power model establishes a connection between the damage threshold metric and the intensity measure (IM).

$$DM = a\ IM^b \quad (3)$$

$$\ln(DM) = \ln a + b \ln(IM) \quad (4)$$

$$\beta_D = \sqrt{\frac{1}{n-2}\sum_{i=1}^{n}\left(\left(\ln(EDV) - \overline{\ln(EDV)}\right)^2\right)} \quad (5)$$

Regression analysis on ln (DM) and intensity measure (IM), we were able to get the regression coefficients a and b that are used in the preceding calculations (Ansari & Agarwal, 2016).

4. Fragility Damage Metrics and Limits

Engineering requirements and structural response characteristics such as pier ductility demand, bearing displacement limit, and pier rotational ductility are used to determine damage limits. The chance of entering a damage stage is represented by a fragility curve and is dependent on the value that is provided for the severity of the ground motion.

The displacement ductility ratio is used to analyses various damage states ranging from minor to collapse, with minor threshold limits ($\Delta y > \Delta_d > \Delta y_1$), moderate threshold limits ($\Delta_2 > \Delta_d > \Delta y$), extensive threshold limits ($\Delta_{c\ max} > \Delta_d > \Delta_2$), and collapse threshold limits ($\Delta_d > \Delta_{cmax}$) being the most prominent.

According to ***Fig. 1***, the yield displacement Δy of the pier is calculated from moment-curvature analysis and Δc_2 represents the displacement ductility under consideration pier portion, while pier displacement ductility at its maximum is indicated by (Δc_2+3), which is taken as concrete strain in pier reaches, Δc 0.002. Because the initial yield displacement is equal to 1, $\Delta y1$ is equal to 1 (Mosleh et al., 2020).

Plastic hinges, which develop as a result of the excessive rotation at the pier, frequently cause bridge damage during earthquakes. It has been demonstrated that bridge piers exposed to lateral seismic loads eventually lose their stiffness and strength. Calculating plastic rotation following the creation of a plastic hinge base on the pier can reveal a damage indication in a pier's rotational ductility (Berry & Eberhard, 2005). To assess the degree of the bridge's damage, the calculated rotational ductility at the plastic hinge component is compared to the rotational ductility requirement threshold for each damage

scenario. In order to get the theoretical moment capacity Mn, the yield curvature φ_y may be calculated by extrapolating the line connecting the initial yield and origin conditions. Difference between the final curvature φ_u and the yield curvature φ_y is the plastic curvature capacity, which is expressed as a φ_p.

$$\varphi_p = \varphi_u - \varphi_y \quad (6)$$

Lp is assumed to have a constant plastic curvature over its corresponding length, which generates a similar φ_p as in the actual bridge structure.

With this equation in mind, we can determine the extension of plastic hinge from the point of contra-flexure to its critical section:

$$Lp = 0.08L + 0.022\, fye * d_{bl} \geq 0.044 fye \quad (7)$$

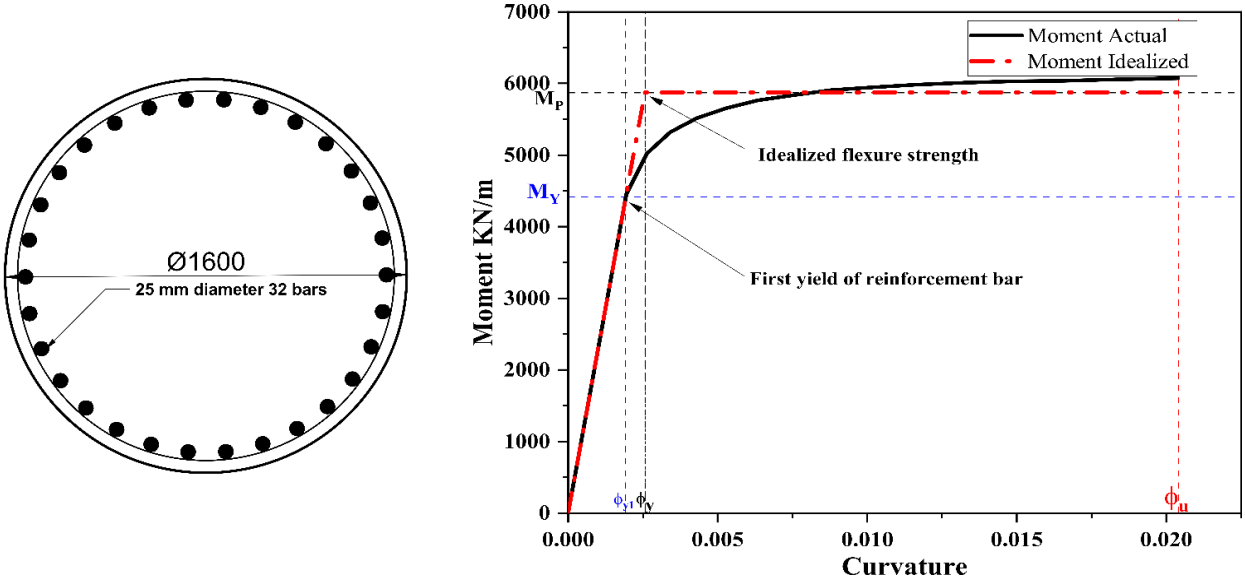

Fig. 1 - Selected pier moment-curvature curve

A bridge collapse will occur when the girder reaches its maximum seat length, which is determined by the superstructure movement from the abutment. As the abutment width and bent size serve as the structure seats, they dictate the circumstances under which this limit state occurs (Elnashai et al., 2004). Due to the deck's longitudinal motion, girders may fall loose from the bearing pads, resulting in structural failure. From AASHTO-LRFD, the minimum seat width will be determined as follows:

$$S = (200 + 0.0017\, L + 0.0067\, H)\,(1 + 0.000125\, \theta^2) \quad (8)$$

In this equation, L represents the deck length in millimeters, S represents the minimum length of support, calculated normal to the centre line of bearing, H is the average height of piers. It is calculated that the minimum seat width is equal to 25%, 50%, 75%, and 100% of the qualifying damage limits for minor, moderate, severe, and collapse damage respectively (Mosleh et al., 2020).

To accurately quantify the vulnerability of the box girder bridge, there are three damage limits that are taken into consideration: (i) the displacement pier ductility that represents the damage to the pier caused by the yielding of the reinforcement bars (DPD); (ii) the rotational pier ductility (RPD) that represents the state of plastic rotation in the bridge pier; and (iii) the maximum girder displacement (MGD) that represents the dislocation of girder from the abutment bearing pads. When determining the seismic vulnerability of a bridge, it is common practice to use a scale with four distinct damage levels. Damage that has been classified as minor, moderate, large, or collapsed is evaluated according to the criteria outlined in HAZUS as depicted in Table 1.

Table 1- Damage metrics and threshold limits

Damage Metrics	Damage Limits			
	Minor	Moderate	Severe	Collapse
	DL1	DL2	DL3	DL4
Displacement ductility of pier (DDP)	1	1.32	1.96	4.96
Rotational Ductility of Pier (RDP)	2.1	6.13	11.27	22.45
Deck displacement (DD)	25% S	50% S	75% S	100% S

5. Configuration of Bridge

For the purpose of the numerical study, a conventional steel box girder bridge with typical RCC circular piers was utilized. According to the bridge data, the spans of the bridge are 32.6, 38.7, 41.2, and 28.2 meters, respectively (Baig et al., 2022). The bridge is a continuous four-span steel box-girder Fig. 2. The two-steel box girder and deck system are part of the steel box girder superstructure, which has a top slab that is 10 meters in length. The actual thickness of the slab is 300 millimeters, and the depth of the box girder is 1.485 meters. It is anticipated that the unconfined concrete strength of the deck will be M45, and the reinforcing steel will be Fe 415 D. Each of the two web plates that make up the steel tub section has a thickness of 20 millimeters and a slope of 4:1. The bottom flange is comprised of a plate that has a width of 1700 mm and a thickness of 50 mm. The bents are supported by a cap beam that has a gradually decreasing rectangular cross section and two circular columns made of reinforced concrete. The bents are held up by reinforced concrete columns that have a diameter of 1.6 meters and a height of 6.6 meters. Each column is constructed from spiral hoops measuring 10 millimeters in diameter and 32 vertical bars measuring 25 millimeters in diameter. These hoops are spaced 150 millimeters apart. The uniaxial stress-strain behavior of unconfined and confined concrete is investigated using concrete with a strength of M45 and the Mander model.

5.1 Finite Element Modelling of Considered Bridge

A three-dimensional model for the structural bridge was generated with the help of the nonlinear finite element software CSI Bridge. Fig. 2 displays the analytical model in its simplified form for the bridge. For the purpose of simulating the superstructure and substructure of the bridge, the lumped mass approach was used (Tondini & Stojadinovic, 2012). In the structural modelling of a steel box girder bridge, elastic beam elements were used to represent the girder, while nonlinear elements were used to simulate the bearings and piers. Rigid links were used to connect the girder and piers with bearings, while fiber-based nonlinear links were used to represents the piers plastic hinge (Hajihashemi et al., 2017). Linear elastic beam-column segments were utilized for the girder, linear link segments were utilized for the bearings and rigid links were utilized for the connection of bearings and girder. The stress-strain relationship of unconfined concrete, confined concrete and longitudinal steel reinforcement is illustrated in Fig. 2, along with the particulars of fiber-based nonlinear components used in the pier sections. The compressive strengths of unconfined concrete are 40 MPa, whereas the compressive strengths of confined concrete are 45 MPa, and the compressive strengths of steel reinforcing yield stress are 415 MPa. Because of the stiff site constraints, the bases of the piers are considered to be fixed and the influence of the soil-interaction is not taken into consideration.

5.2 Model for Bearings

In CSI Bridge, bearings are depicted as linear connections that connect one joint to the superstructure and the other to the bending. There are six degrees of freedom in deformation: axial, shear, torsion, and pure bending. A link element operates as a single element made up of six springs and is a joint supported spring. As shown in Fig. 2, the roller abutment model is given at both ends of the girder and comprises of a basic boundary condition module that provides single-point restrictions against vertical displacement (vertical support). This model may be used to provide a lower-bound estimate of the bridge's longitudinal and transverse resistance using a pushover study. At the intermediate bends, steel rocker bearings are fitted. The development of plastic hinges and the ductility capability of the column bents dominate the reaction of this basic bridge model.

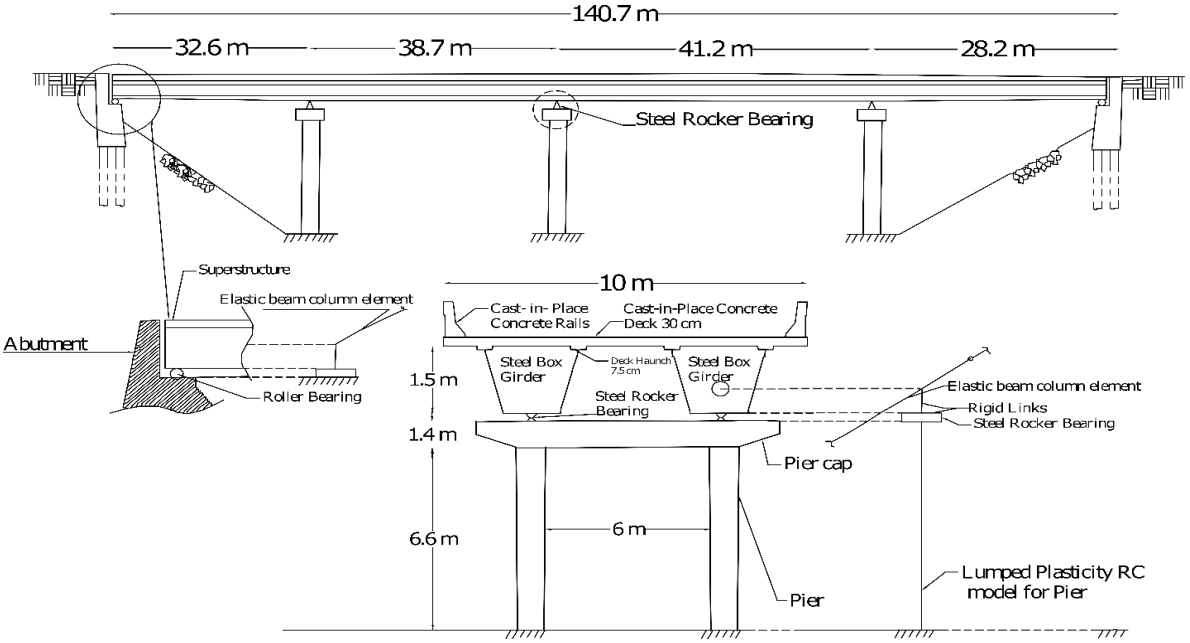

Fig. 2 - Cross-sectional view of considered steel box girder bridge

6. Selection of Ground Motions

The ground motion data are the most inherent aspect of developing fragility curves. It is crucial to choose an acceptable ground motion and scale the ground motions before attempting to construct this curve (Banerjee & Shinozuka, 2007). The ground motion close to a fault is characterized by a high energy velocity. It is distinguished by its pulse-like waveforms, long period, as well as unique high peak values (Yang et al., 2021). The ground motions that concentrate the majority of the ground motions created by the radiated seismic energy are referred to be "pulse-like" and they are characterized by the presence of a full-cycle velocity pulse at the beginning of the waveform.

The selection of near-field recordings was based on the presence of a high-amplitude and periodic velocity pulse, as well as the distance from the fault that the record was recorded. For the purpose of the study, each ensemble was given a selection of 10 unique ground motions with peak ground accelerations (PGAs) ranging from 0.1 to 1.2 g. Each ground motion was scaled to PGAs ranging from 0.1 to 1.2 g, with an interval of 0.1 g, in order to execute the incremental dynamic analysis that was previously stated.

Fling-step is involved with permanent tectonic displacement, which is represented by a full sinusoidal pulse in the time history of acceleration and a half sinusoidal pulse in the velocity time history (Hamidi Jamnani et al., 2013). Raw fling-step recordings must be processed in order to provide authentic tectonic deformation. The impact of fling-step is investigated in this research using raw data from the Chi-Chi earthquake

Table ***3***. The processed data from Bhandari were chosen because they had to meet the following criteria: a magnitude (Mw) between 7 and 7.6, a peak ground displacement (PGD) between 100 and 230 cm, and a radius (Rjb) of less than 15 kilometers (Bhandari et al., 2019). For incremental dynamic analysis, the PEER Center seismic records for forward directivity datasets with Rjb less than 10 km, magnitude (Mw) between 6 and 7.5 are utilized depicted in Table 2. The structures were subjected to the accelerogram of the relevant earthquake, with no scaling coefficients for the standard design spectrum Fig. 3.

Table 2 - Records of forward directivity earthquakes

Record	Year	Earthquake	Mag	Station	PGA (g)	Rib (Km)	PGV (m/s)	PGD m
1	1979	Imperial	6.48	Brawley	0.16	8.54	0.36	0.256
2	1991	Cape Mendocino	7.02	Bunker Hill	0.18	8.49	0.68	0.38
3	1980	Irpinia	6.88	Bagnoli	0.13	8.14	0.23	0.13
4	1980	Irpinia	6.9	Surnow	0.23	6.78	0.36	0.14

5	1979	Imperial	6.48	EC County	0.21	7.31	0.38	0.169
6	1989	Loma Prieta	6.89	Gilroy	0.29	10.27	0.44	0.98
7	1994	Northridge	6.69	Jensen	0.41	0.00	1.12	0.45
8	1992	Landers	7.28	Lucerne	0.73	2.19	1.34	1.13
9	1995	Kobe Japan	6.86	Port Island	0.35	3.31	0.91	0.40
10	1995	Kobe Japan	6.86	Taka tori	0.62	1.46	1.22	0.41

Table 3 - Records of fling step earthquakes

Record.	Year	Earthquake	Mag	Station	PGA (g)	Rjb (Km)	PGV (m/s)	PGD m
1	1999	Chi-Chi EW	7.6	TCU 072	0.46	7.90	0.83	2.1
2	1999	Chi-Chi	7.6	TCU 067	0.48	1.10	0.95	1.81
3	1999	Chi-Chi NS	7.6	TCU 072	0.36	7.90	0.67	2.45
4	1999	Chi-Chi	7.6	TCU 075	0.32	3.40	1.12	1.64
5	1999	Chi-Chi	7.6	TCU 074	0.59	13.80	0.69	1.93
8	1999	Chi-Chi	7.6	TCU 089	0.34	8.30	0.45	1.4
6	1999	Chi-Chi	7.6	TCU 076	0.33	3.20	0.66	1.02
7	1999	Chi-Chi	7.6	TCU 049	0.27	3.30	0.55	1.21
9	1999	Chi-Chi	7.6	TCU 082	0.22	7.60	0.51	1.43
10	1999	Kocaeli	7.4	Sarkaya	0.41	3.20	0.83	2.06

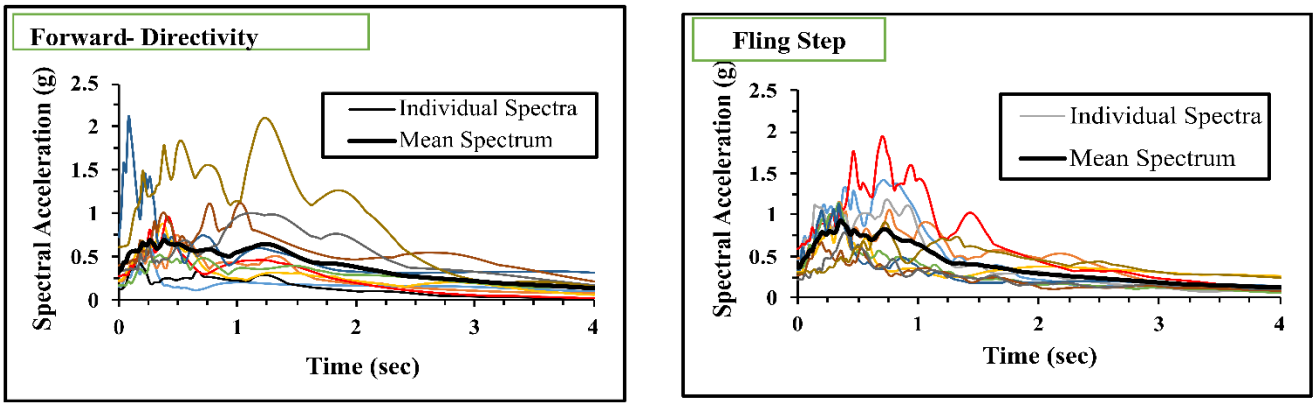

Fig. 3 - Pseudo acceleration response spectra (5% damping) for forward directivity and fling step records

7. Results and Discussions

CSI Bridge is used to conduct nonlinear dynamic assessments of the bridge and calculate the seismic behavior of the selected bridge model. A lognormal distribution of structural reactions is described based on displacement pier ductility, rotational pier ductility and maximum girder displacement. Each set of earthquake records is made up of ten measurements of ground motion that range from 0.1g to 1.2g. The fragility curves of the steel box girder bridge for various damage levels were created by calculating the likelihood that a specific damage limit condition will be reached.

Fig. 4 (a-b) shows the typical IDA curve for displacement pier ductility for both forward directivity and fling step seismic records for PGA of 0.1 g to 1.2 g.

As the Fig. 4 shows, the response displacement pier ductility for the forward directivity records is much higher than fling step. The bridge begins in the collapse damage limit at 0.42g for the forward directivity records and 0.58g for the fling step records. Also, Fig. 4 shows that at the design level earthquake which is 0.2 g (Pga), the difference in displacement pier ductility requirements between forward directivity and fling step records are not significant. At extreme level earthquake which is 0.4g (Pga), this difference is significant. Fig. 4 shows that the difference between the pier ductility requirements for forward directivity and the fling-step effect is more noticeable when PGA = 0.4 g and more. The maximum force and reaction

are developed by the Kobe ground motion under forward directivity and TCU082 under the fling step record. Due of the significant energy pulses reported in earthquake records at each PGA levels, ductility requirements exist more in the forward directivity records. Also, when fling step records are compared to forward directivity, the amplification factor is 2.64. Due to the "fling-step" effect, sudden displacement occurred due to tectonic permanent ground offset happens all at once and the response is still in collapse condition after 0.6g.

The inelastic behavior of the bridge pier is investigated by predicting the formation of plastic hinges in the bottom of the bridge pier under forward directivity and fling step earthquake. Thus, according Caltrans, there are various levels of performance for plastic hinges (B, IO, LS, CP). The bridge's reaction is calculated by dividing the amount of plastic rotation at the hinge by the amount of yield rotation at the pier. Fig. 5 shows that there is no hinge formation, and the rotational ductility is within the allowable range for the fling step earthquakes at 0.2g. However, for forward directivity there is plastic rotation and the formation of a plastic hinge develops at 0.2 g. When the Peak ground acceleration is 0.4g or more the pier suffered more plastic rotations due to forward directivity and fling-step earthquakes which pronounced more collapse to the bridge.

As a result, for the near fault earthquakes, the seismic design of bridges necessitates appropriate requirements on ductility limits and rotation of plastic hinges. Some records, such as the Northridge and TCU075, produce a significant rise in rotational ductility demands as the PGA value rises. The plastic rotation increases abruptly when a PGA value is greater than 0.6 g. In most situations, substantial plastic hinge rotation occurs after PGA = 0.5 g for different ensembles of earthquakes. Fig. 5 shows that the fluctuation of plastic rotation is linear, and the bridge is in the linear stage up to PGA = 0.3 g and then becomes nonlinear after PGA = 0.4 g.

Fig. 6 shows the maximum girder displacement responses and their corresponding median values for different groups of earthquakes. The peak girder displacement for the forward directivity are roughly 2.42 times larger than those for the fling step records. The amplifying response for the forward directivity impulsive ground motion is shown to be 2.42 as compared to the fling-step effect. This indicates that the forward directivity impact is more significant than the fling-step effect when it comes to the reaction of the bridge girder displacement. It can be shown in (**Error! Reference source not found.**) that the bridge enters a condition of collapse with a horizontal acceleration of 0.52 g in the forward directivity and 0.78 g in the fling step ground motions.

This data was utilized in regression analysis to develop probabilistic damage models (PSDM) in the event of earthquakes [38]. They demonstrate the dispersion of bridge response data with ten values (particularly for a damage metrics) in a stripe-based format. Logarithmic median and standard deviation required to define the lognormal distribution (Eq. (1), were obtained using a linear regression analysis of ln (peak ground acceleration) on ln (damage metrics).

Equation (3) and (4) were used to calculate the median of each threshold damage level value. Displacement pier ductility, rotational pier ductility and maximum girder displacement data are shown for varied ground motions in the PSDMs shown in Fig. 7. Different demand metrics and intensities of earthquakes are represented in probabilistic seismic demand models Table 4.

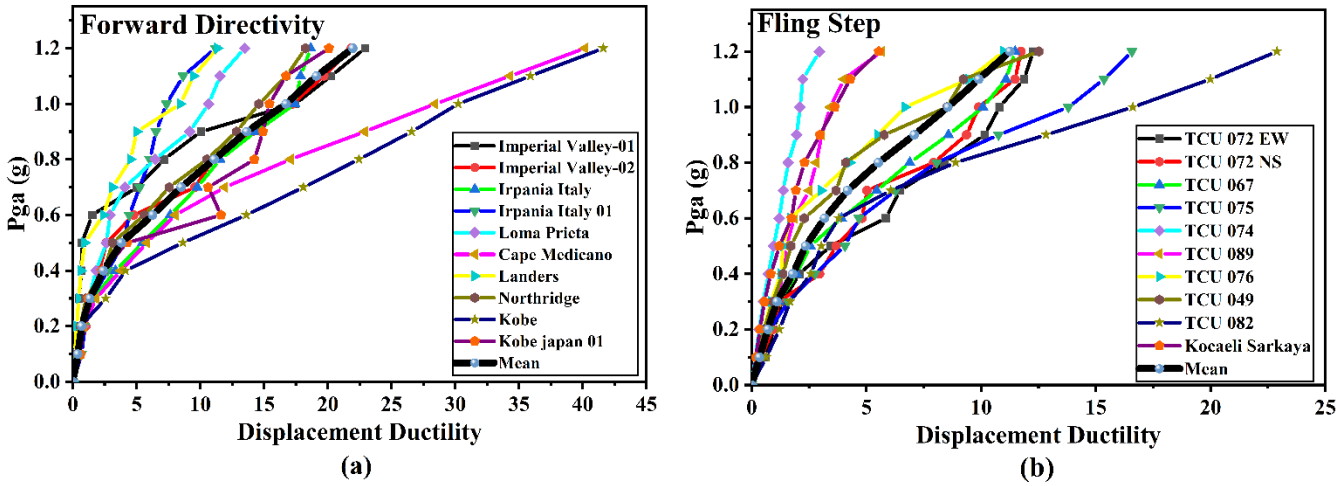

Fig. 4 - Displacement pier ductility IDA curves for: (a) forward directivity; (b) fling step

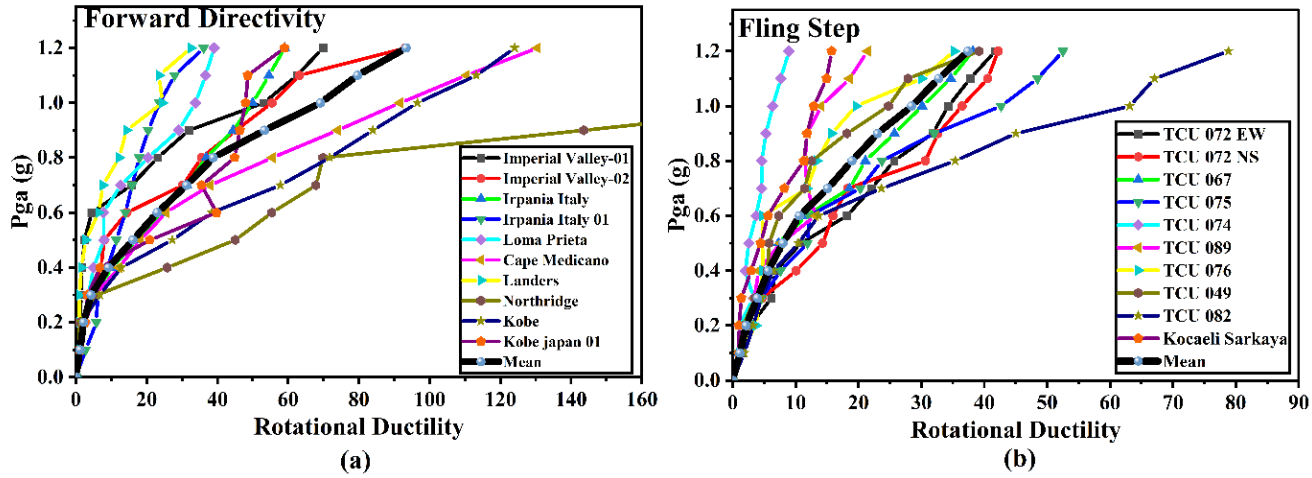

Fig. 5 - Rotational pier ductility IDA curves for: (a) forward directivity; (b) fling step

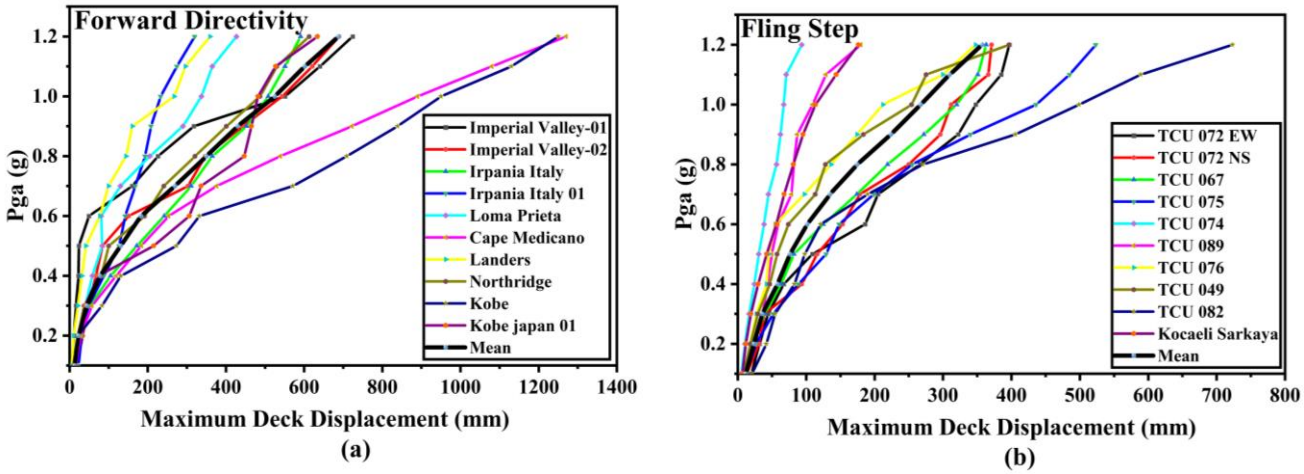

Fig. 6 - Maximum girder displacement IDA curves for: (a) forward directivity; (b) fling step

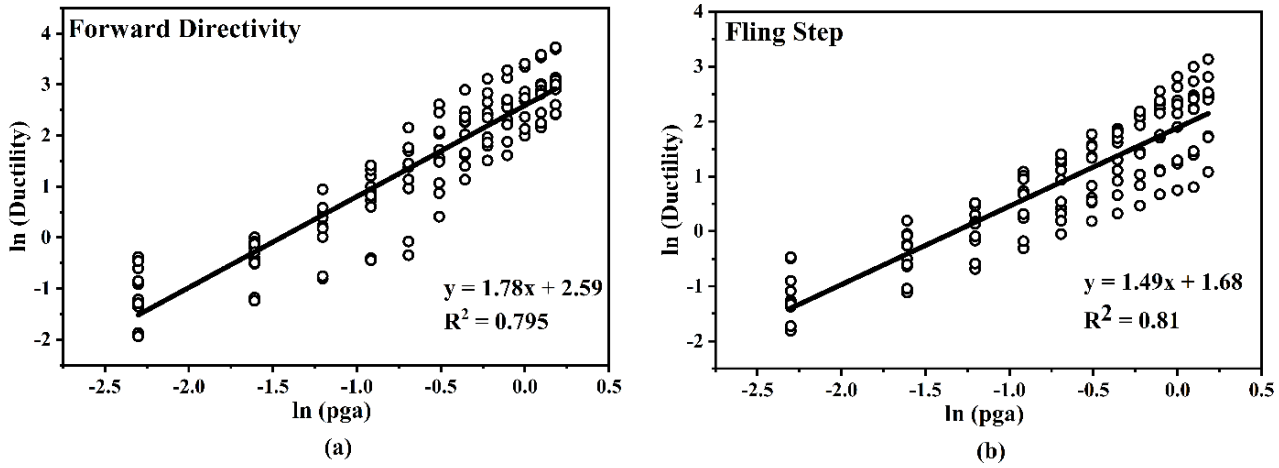

Fig. 7 - Probabilistic seismic demand model for displacement pier ductility for: (a) forward directivity; (b) fling step

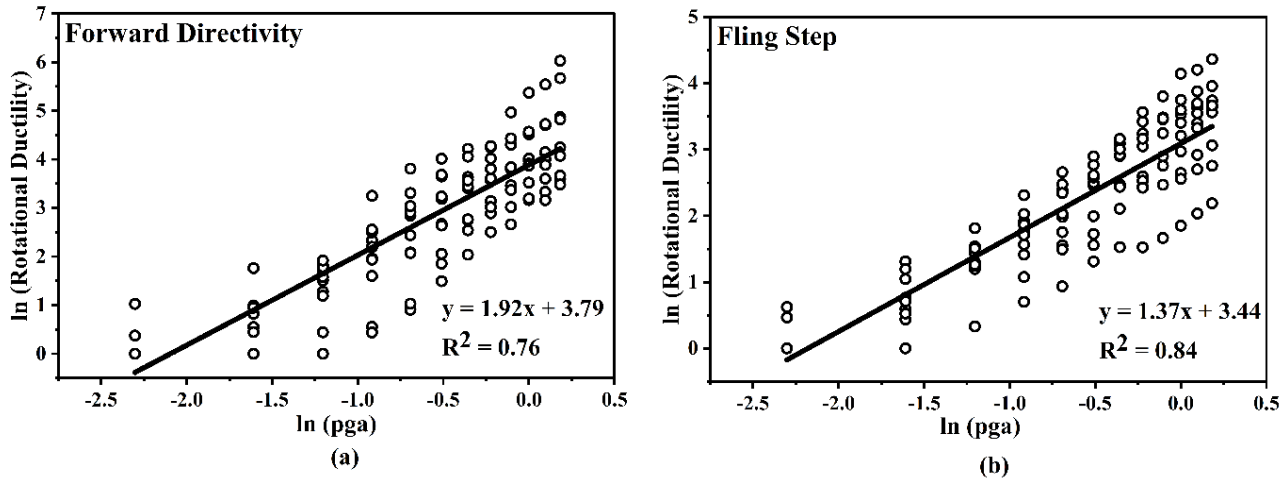

Fig. 8 - Probabilistic seismic demand model for rotational pier ductility for: (a) forward directivity; (b) fling step

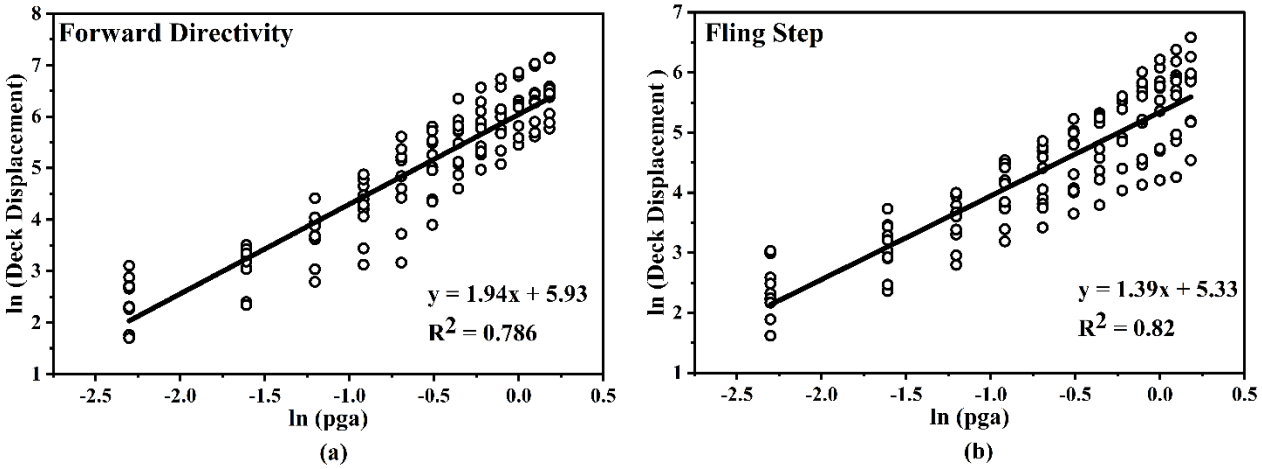

Fig. 9 - Probabilistic seismic demand model for girder displacement for: (a) forward directivity; (b) fling step

Table 4 - Probabilistic seismic demand model for various demand metrics

Damage Measure	Type of earthquake	Response	Demand Model	β_D	R^2
Displacement pier ductility	Forward Directivity	ln (DPD)	ln 13.32 + 1.68 ln (Pga)	1.36	0.795
Girder displacement		ln (MGD)	ln 379.98 + 1.94 ln (Pga)	1.28	0.786
Rotational pier ductility		ln (RPD)	ln 44.25 + 1.92 ln (Pga)	1.49	0.76
Displacement pier ductility	Fling Step	ln (DPD)	ln 5.36 + 1.5 ln (Pga)	1.27	0.81
Girder displacement		ln (MGD)	ln 208.6 + 1.4 ln (Pga)	1.23	0.82
Rotational pier ductility		ln (RPD)	ln 31.2 + 1.37 ln (Pga)	1.25	0.84

7.1 Fragility Curve Comparison

Fig. 10-12 presents the fragility curves for two ensembles of near fault earthquakes: (a) forward directivity and (b) fling Step effect. These curves represent the various threshold damage limits associated with various damage metrics (minor,

moderate, severe and collapse) and are presented for various threshold damage limit states (

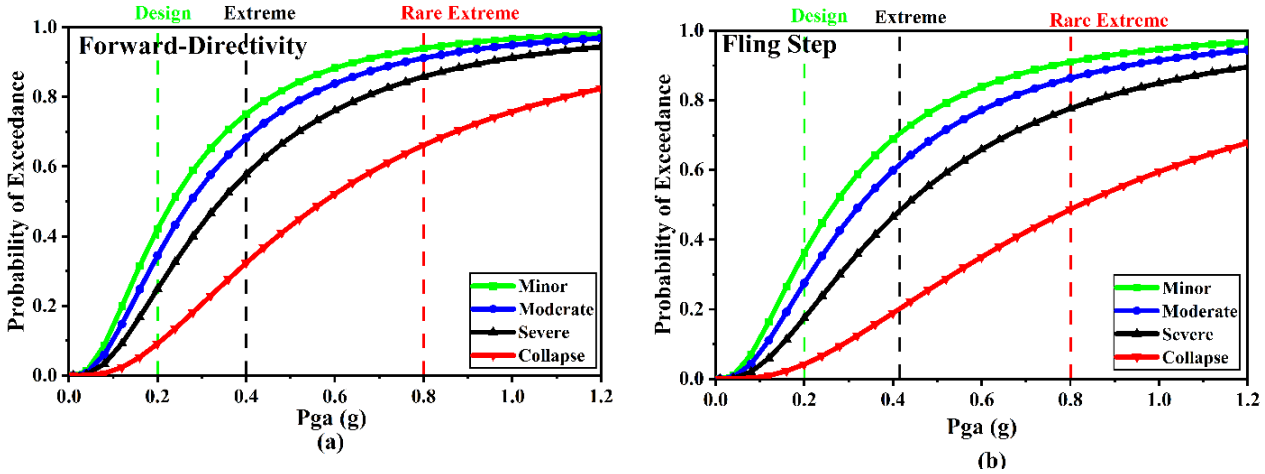

Fig. *10* - **Displacement pier ductility fragility curves for various damage limit for: (a) forward directivity; (b) fling step**

-14). Due to the higher probability of exceedance, the bridge is more susceptible to damage from forward directivity records than the fling step seismic events. The probability of exceedance varies much less across different ensembles of ground movements for low-level damage states that are associated with a variety of damage metrics. The difference in the probability of exceedance becomes significant as the condition of damage increases from severe to complete collapse.

The POE for various groups of earthquakes was examined at three distinct PGA levels: 0.2g (design), 0.4g (extreme) and 0.8g (rare extreme). From the various ensembles of earthquakes that were examined as part of this study, the fragility curves for displacement pier ductility, rotational pier ductility, and maximum girder displacement are shown in Fig. 10. The POE for forward directivity ground motion is large at higher damage stages, such as moderate to severe, even at smaller PGA values, such as 0.2g (design).The earthquake with forward directivity has the greatest POE in terms of displacement pier ductility, with 23.8 % at design level, 57.2 % at extreme level and 84.2 % at rare extreme in the severe damage limit (DL3) as depicted in Fig. 10 (a), while the POE will be 8.7 % at design level, 29.8 % at extreme level, and 62.4 % at rare extreme level in the stage of collapse damage limit (DL4). The fling step records has the highest POE for displacement pier ductility, which is 16.6 % at design level, 44.3 % at extreme, and 76.2 % at rare extreme in the severe damage limit (DL3) while 3 % at design, 17 % at extreme, and 46.2 % at rare extreme in the collapse damage limit as shown in Fig. 10 (b). Even at the phases of significant catastrophic collapse damage, the probability of fling step records remains rather high even as PGA levels rise.

The (POE) for maximum girder displacement under forward directivity is 24 % at 0.4g and 54 % at 0.8g in the severe damage limit and it is 18 % at 0.4g and 48 % at 0.8g in the severe damage limit depicted in Fig. 12. In the collapse limit the POE for forward directivity lies between 3% at design level to 44% at rare extreme level. The maximum girder displacement for fling step earthquakes in the levels of damage that are minor, moderate, severe, and collapse it is above 70 % in the degree of damage that in forward directivity.

Because the rotational pier ductility and displacement pier ductility curves for various types of earthquakes are equivalent and display similar patterns, they are not discussed further here.

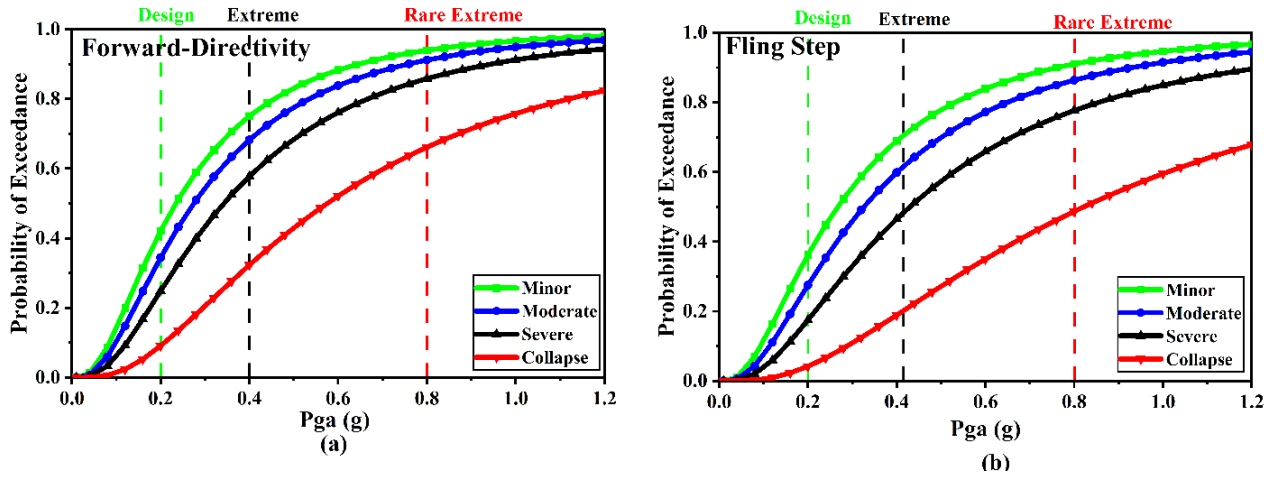

Fig. 10 - Displacement pier ductility fragility curves for various damage limit for: (a) forward directivity; (b) fling step

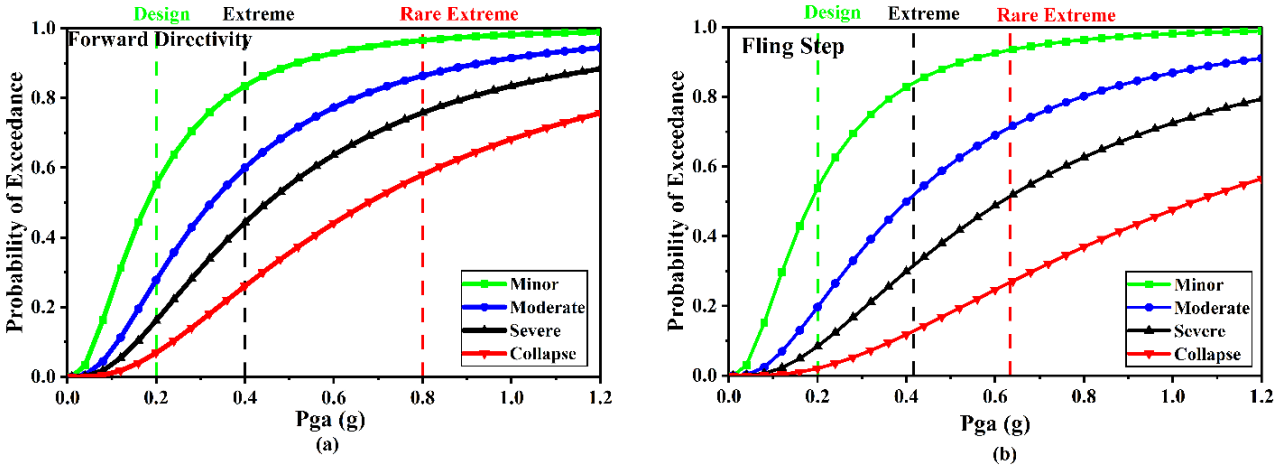

Fig. 11 - Rotational pier ductility fragility curves for various damage limit for: (a) forward directivity; (b) fling step

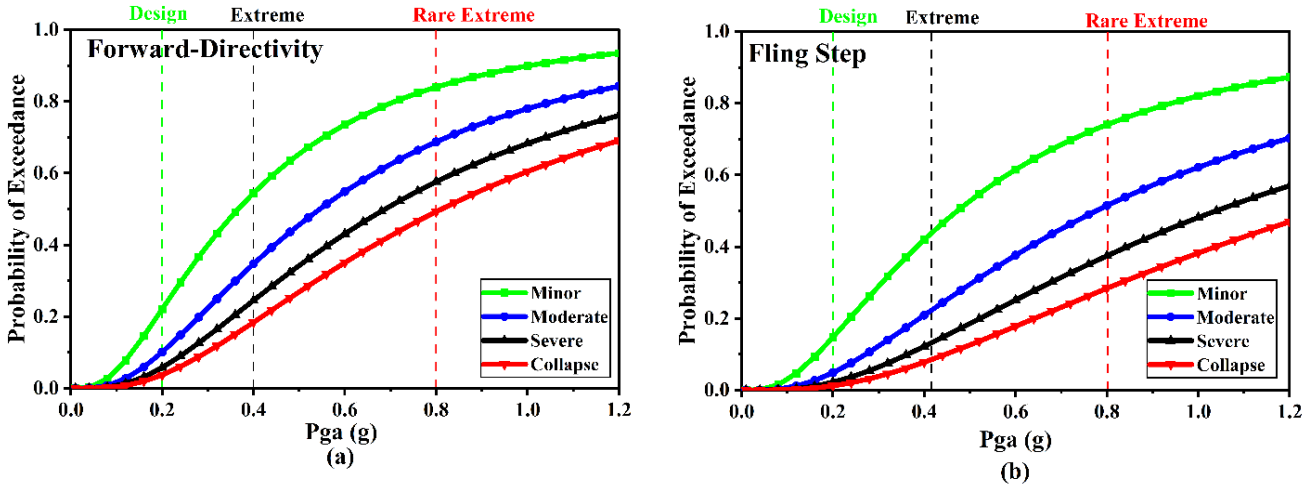

Fig. 12 - Girder displacement fragility curves for various damage limit for: (a) forward directivity; (b) fling step

8. Conclusions

The present work investigates the fragility analysis and probabilistic seismic risk assessment of steel box girder bridges under near fault earthquakes. The ensemble of earthquakes used to investigate seismic sensitivity is made up of two separate sets: (1) forward directivity and (2) fling-step ground motion. The incremental dynamic analysis approach is used to generate

a set of seismic responses that includes a variety of demand metrics such as displacement pier ductility, rotational pier ductility and maximum girder displacement. The incremental dynamic analysis is based on a set of 10 ground motion data points for each type of earthquake. By using regression analysis, a probabilistic seismic demand model was developed, as well as fragility curves with four damage phases: minor, moderate, severe, and collapse. The following are the primary findings of the study:

- The numerical findings reveal that pier in the forward directivity earthquakes damage the steel box girder bridges more than fling step ground motion ensembles.
- When the bridge is exposed to forward directivity ground motion, the ductility requirement in the pier becomes significantly larger while fling step also damages the bridge after 0.4g.
- Forward directivity ground motions increase bridge pier and girder forces. Pulse-like feature in forward directivity earthquake increase bridge girder displacement after 0.5g pga level. This combination causes a high exceedance probability in all damage states and damage indices.
- It has been observed that there is a significant difference in the exceedance probability between forward directivity and fling step, and this difference is especially noticeable at high PGA levels (> 0.4g), as well as at the severe and collapse damage stages.
- The fragility median indicates that at lower PGA levels, there is only a minor deviation in the fragility curve due to variability in the first two damage stages, but as PGA levels increase this variability becomes more noticeable at high damage limits.
- According to the findings, the three sensitive damage assessments that have a high exceedance probability in all damage states are displacement pier ductility, rotational pier ductility and girder displacement. As a consequence of this, it is possible to propose that the design of the bridge takes into account all three demand measures, in particular during earthquakes characterized by forward directivity and fling-step.
- According to the findings of the study, the parameters of earthquake sources have a significant influence on the structural integrity of bridges. As a direct consequence of this, careful consideration must be given to ground motions whenever a bridge's seismic risk is being evaluated.

Acknowledgement

The authors would like to thank Department of Civil Engineering, Jamia Millia Islamia University, New Delhi, 110025, India for allowing to conduct this research.

References

Ansari, M. I., & Agarwal, P. (2016). Categorization of Damage Index of Concrete Gravity Dam for the Health Monitoring after Earthquake. *Journal of Earthquake Engineering*, *20*(8), 1222–1238. https://doi.org/10.1080/13632469.2016.1138167

Baig, M. A., Ansari, I., Islam, N., & Umair, M. (2022). Materials Today : Proceedings Damage assessment of circular bridge pier incorporating high-strength steel reinforcement under near-fault ground motions. *Materials Today: Proceedings*, *xxxx*. https://doi.org/10.1016/j.matpr.2022.04.964

Baker, J. W., & Cornell, C. A. (2008). Vector-valued intensity measures incorporating spectral shape for prediction of structural response. In *Journal of Earthquake Engineering* (Vol. 12, Issue 4). https://doi.org/10.1080/13632460701673076

Banerjee, S., & Shinozuka, M. (2007). Nonlinear static procedure for seismic vulnerability assessment of bridges. *Computer-Aided Civil and Infrastructure Engineering*, *22*(4), 293–305. https://doi.org/10.1111/j.1467-8667.2007.00486.x

Berry, M. P., & Eberhard, M. O. (2005). Practical Performance Model for Bar Buckling. *Journal of Structural Engineering*, *131*(7), 1060–1070. https://doi.org/10.1061/(asce)0733-9445(2005)131:7(1060)

Bhagat, S., Wijeyewickrema, A. C., & Subedi, N. (2021). Influence of Near-Fault Ground Motions with Fling-Step and Forward-Directivity Characteristics on Seismic Response of Base-Isolated Buildings. *Journal of Earthquake Engineering*, *25*(3), 455–474. https://doi.org/10.1080/13632469.2018.1520759

Bhandari, M., Bharti, S. D., Shrimali, M. K., & Datta, T. K. (2019). Seismic Fragility Analysis of Base-Isolated Building Frames Excited by Near- and Far-Field Earthquakes. *Journal of Performance of Constructed Facilities*, *33*(3), 04019029. https://doi.org/10.1061/(asce)cf.1943-5509.0001298

Billah, A. H. M. M., Alam, M. S., & Bhuiyan, M. A. R. (2013). Fragility Analysis of Retrofitted Multicolumn Bridge Bent

Subjected to Near-Fault and Far-Field Ground Motion. *Journal of Bridge Engineering*, *18*(10), 992–1004. https://doi.org/10.1061/(asce)be.1943-5592.0000452

BOLT, B. (2004). Seismic input motions for nonlinear structural analysis. *ISET Journal of Earthquake Technology*, *41*(2), 223–232.

Burks, L. S., & Baker, J. W. (2016). A predictive model for fling-step in near-fault ground motions based on recordings and simulations. *Soil Dynamics and Earthquake Engineering*, *80*, 119–126. https://doi.org/10.1016/j.soildyn.2015.10.010

Elnashai, A. S., Borzi, B., & Vlachos, S. (2004). Deformation-based vulnerability functions for RC bridges. *Structural Engineering and Mechanics*, *17*(2), 215–244. https://doi.org/10.12989/sem.2004.17.2.215

Ertuncay, D., Malisan, P., Costa, G., & Grimaz, S. (2021). Impulsive Signals Produced by Earthquakes in Italy and Their Potential Relation with Site Effects and Structural Damage. *Geosciences*, *11*(6), 261. https://doi.org/10.3390/geosciences11060261

Fariborz, N.-A., & Vahid, L. S. (2004). Development of Fragility and Reliability Curves for Seismic Evaluation of a Major Prestressed Concrete. *13 Th World Conference on Earthquake Engineering*, *1351*, 1–11.

Federal Emergency Management Agency. (2020). Hazus Earthquake Model Technical Manual . *Federal Emergency Management Agency*, *October*, 1–436.

Gentile, R., & Galasso, C. (2021). Accounting for directivity-induced pulse-like ground motions in building portfolio loss assessment. *Bulletin of Earthquake Engineering*, *19*(15), 6303–6328. https://doi.org/10.1007/s10518-020-00950-9

Hajihashemi, A., Pezeshk, S., & Huff, T. (2017). Comparison of Nonlinear Static Procedures and Modeling Assumptions for the Seismic Design of Ordinary Bridges. *Practice Periodical on Structural Design and Construction*, *22*(2), 04016022. https://doi.org/10.1061/(asce)sc.1943-5576.0000309

Hamidi, H., Karbassi, A., & Lestuzzi, P. (2020). Seismic response of RC buildings subjected to fling-step in the near-fault region. *Structural Concrete*, *21*(5), 1919–1937. https://doi.org/10.1002/suco.201900028

Hamidi Jamnani, H., Karbassi, A., & Lestuzzi, P. (2013). Fling-step effect on the seismic behavior of high-rise RC buildings during the Christchurch earthquake. *2013 NZSEE Conference*, *Xx*.

Lo Monte, F., Pozzuoli, C., Mola, E., & Mola, F. (2018). Seismic Vulnerability Assessment and Retrofitting Design of a Multispan Highway Bridge: Case Study. *Journal of Bridge Engineering*, *23*(2), 05017016. https://doi.org/10.1061/(asce)be.1943-5592.0001148

Ma, H. Bin, Zhuo, W. D., Yin, G., Sun, Y., & Chen, L. B. (2016). A Probabilistic Seismic Demand Model for Regular Highway Bridges. *Applied Mechanics and Materials*, *847*(Im), 307–318. https://doi.org/10.4028/www.scientific.net/amm.847.307

Mangalathu, S., Jeon, J.-S., & Jiang, J. (2019). Skew Adjustment Factors for Fragilities of California Box-Girder Bridges Subjected to near-Fault and Far-Field Ground Motions. *Journal of Bridge Engineering*, *24*(1), 04018109. https://doi.org/10.1061/(asce)be.1943-5592.0001338

Mena, B., & Mai, P. M. (2011). Selection and quantification of near-fault velocity pulses owing to source directivity. *Georisk*, *5*(1), 25–43. https://doi.org/10.1080/17499511003679949

Mimoglou, P., Psycharis, I. N., & Taflampas, I. M. (2017). Determination of the parameters of the directivity pulse embedded in near-fault ground motions and its effect on structural response. *Computational Methods in Applied Sciences*, *44*, 27–48. https://doi.org/10.1007/978-3-319-47798-5_2

Moniri, H. (2017). Investigation of Fling-Step Effect on Mid-Rise R / C Buildings Subjected To Near Source Strong Motion. *16th World Conference on Earthquake Engineering, Santiago, Chile, 9-13 January*.

Mosleh, A., Jara, J., Razzaghi, M. S., & Varum, H. (2020). Probabilistic Seismic Performance Analysis of RC Bridges. *Journal of Earthquake Engineering*, *24*(11), 1704–1728. https://doi.org/10.1080/13632469.2018.1477637

Muntasir Billah, A. H. M., & Shahria Alam, M. (2015). Seismic fragility assessment of highway bridges: a state-of-the-art review. *Structure and Infrastructure Engineering*, *11*(6), 804–832. https://doi.org/10.1080/15732479.2014.912243

Nicknam, A., Barkhordari, M. A., Hamidi Jamnani, H., & Hosseini, A. (2014). Probable contribution of fling-step effect on the response spectra at near source site. *Journal of Vibroengineering*, *16*(1), 334–340.

Sengupta, A., Quadery, L., Sarkar, S., & Roy, R. (2016). Influence of Bidirectional Near-Fault Excitations on RC Bridge Piers. *Journal of Bridge Engineering*, *21*(7), 04016034. https://doi.org/10.1061/(asce)be.1943-5592.0000836

Somerville, P. G., Smith, N. F., Graves, R. W., & Abrahamson, N. A. (1997). Modification of empirical strong ground motion attenuation relations to include the amplitude and duration effects of rupture directivity. *Seismological Research Letters*, *68*(1), 199–222. https://doi.org/10.1785/gssrl.68.1.199

Tondini, N., & Stojadinovic, B. (2012). Probabilistic seismic demand model for curved reinforced concrete bridges. *Bulletin of Earthquake Engineering*, *10*(5), 1455–1479. https://doi.org/10.1007/s10518-012-9362-y

Yadav, K. K., & Gupta, V. K. (2017). Near-fault fling-step ground motions: Characteristics and simulation. *Soil Dynamics*

and Earthquake Engineering, *101*(December 2015), 90–104. https://doi.org/10.1016/j.soildyn.2017.06.022

Yang, J., Li, P., Jing, H., & Gao, M. (2021). Near-Fault Ground Motion Influence on the Seismic Responses of a Structure with Viscous Dampers considering SSI Effect. *Advances in Civil Engineering*, *2021*. https://doi.org/10.1155/2021/6649124

Zeng, W., Zhuo, W., & Briseghella, B. (2019). Probabilistic seismic demand model for regular bridges based on the modified Park-Ang damage index. *IOP Conference Series: Earth and Environmental Science*, *218*(1). https://doi.org/10.1088/1755-1315/218/1/012084